Characterization of Redox States of Ru(OH2)(Q)(tpy)(2+) (Q=3,5-di-tert-butyl-1,2-benzoquinone, tpy=2,2 ':6 ',2 ''-terpyridine) and Related Species through Experimental and Theoreti...

ARTICLE *in* INORGANIC CHEMISTRY · JUNE 2009

Impact Factor: 4.76 · DOI: 10.1021/ic900057y · Source: PubMed

7 AUTHORS, INCLUDING:

Jonathan Rochford
University of Massachusetts Boston
31 PUBLICATIONS **1,066** CITATIONS
SEE PROFILE

Dmitry E Polyansky
Brookhaven National Laboratory
41 PUBLICATIONS **695** CITATIONS
SEE PROFILE

Etsuko Fujita
Brookhaven National Laboratory
175 PUBLICATIONS **5,364** CITATIONS
SEE PROFILE

James T Muckerman
Brookhaven National Laboratory
237 PUBLICATIONS **6,440** CITATIONS
SEE PROFILE

Inorg. Chem. **2009**, *48*, 4372−4383

Characterization of Redox States of $Ru(OH_2)(Q)(tpy)^{2+}$ (Q = 3,5-di-*tert*-butyl-1,2-benzoquinone, tpy = 2,2′:6′,2″-terpyridine) and Related Species through Experimental and Theoretical Studies

Ming-Kang Tsai,[†] Jonathan Rochford,[†] Dmitry E. Polyansky,[†] Tohru Wada,[§] Koji Tanaka,[§] Etsuko Fujita,*[,†] and James T. Muckerman*[,†,‡]

Chemistry Department, Brookhaven National Laboratory, Upton, New York 11973-5000, Center for Functional Nanomaterials, Brookhaven National Laboratory, Upton, New York 11973-5000, and Coordination Chemistry Laboratories, Institute for Molecular Science, Okazaki, Aichi 444-8787, Japan

Received January 12, 2009

The redox states of $Ru(OH_2)(Q)(tpy)^{2+}$ (Q = 3,5-di-*tert*-butyl-1,2-benzoquinone, tpy = 2,2′:6′,2″-terpyridine) are investigated through experimental and theoretical UV-vis spectra and Pourbaix diagrams. The electrochemical properties are reported for the species resulting from deprotonation and redox processes in aqueous solution. The formal oxidation states of the redox couples in the various intermediate complexes are systematically assigned using electronic structure theory. The controversy over the electronic assignment of ferromagnetic vs. antiferromagnetic coupling is investigated through comparison of ab initio methods and the broken-symmetry density functional theory (DFT) approach. The various pK_a values and reduction potentials, including the consideration of proton-coupled electron-transfer (PCET) processes, are calculated, and the theoretical version of the Pourbaix diagram is constructed in order to elucidate and assign several previously ambiguous regions in the experimental diagram.

Introduction

Nature has devised an elegant way of converting solar irradiation into chemical energy in green plants by reducing CO_2 to carbohydrates and oxidizing water to O_2. The oxygen-evolving center (OEC) in Photosystem II with the Mn_3CaO_4 cluster is capable of generating about 1000 O_2 molecules per second,[1] while artificial binuclear transition-metal catalysts, including the extensively investigated blue dimer,[2] $(bpy)_2(H_2O)M{-}O{-}M(OH_2)(bpy)_2$, produce O_2 molecules much more slowly and are unstable.[2−4] Tanaka and coworkers have reported water oxidation catalytic activity of a novel dinuclear Ru complex, $[Ru_2(OH)_2(3,6\text{-}Bu_2Q)_2(btpyan)](SbF_6)_2$ (3,6-Bu_2Q = 3,6-di-*tert*-butyl-1,2-benzoquinone, btpyan = 1,8-bis(2,2′:6′,2″-terpyrid-4′-yl)anthracene) in which two $Ru(OH)(3,6\text{-}Bu_2Q)(tpy)^+$ molecules are strategically connected by an anthracene bridge to make an O−O bond without a steric constraint.[5] This catalyst also contains redox-active quinone ligands that can become semiquinone (SQ) or catecholate (Cat). While the OEC and all previous man-made catalysts investigated involve high oxidation states of the M=O species formed via proton-coupled electron-transfer (PCET) reactions before forming an O−O bond, our preliminary gas-phase density functional theory (DFT) calculations on the Tanaka catalyst showed the intriguing property of retaining a predominantly Ru(II) oxidation state throughout the entire catalytic cycle.[6]

A thorough understanding of the monomer of Tanaka's binuclear Ru catalyst as a simple but informative model might provide insights into the catalytic mechanism of the dimer. In comparison with the dimer, the monomer is more soluble and convenient for electrochemical measurements, and the size of the monomer is more amenable to detailed

* To whom correspondence should be addressed. E-mail: fujita@bnl.gov (E.F.), muckerma@bnl.gov (J.T.M.).
[†] Chemistry Department.
[§] Institute for Molecular Science.
[‡] Center for Functional Nanomaterials.

(1) Ruttinger, W.; Dismukes, G. C. *Chem. Rev.* **1997**, *97*, 1.
(2) Gilbert, J. A.; Eggleston, D. S.; Murphy, W. R.; Geselowitz, D. A.; Gersten, S. W.; Hodgson, D. J.; Meyer, T. J. *J. Am. Chem. Soc.* **1985**, *107*, 3855.
(3) Chronister, C. W.; Binstead, R. A.; Ni, J. F.; Meyer, T. J. *Inorg. Chem.* **1997**, *36*, 3814.
(4) Hurst, J. K. *Coord. Chem. Rev.* **2005**, *249*, 313.
(5) Wada, T.; Tsuge, K.; Tanaka, K. *Inorg. Chem.* **2001**, *40*, 329.
(6) Muckerman, J. T.; Polyansky, D. E.; Wada, T.; Tanaka, K.; Fujita, E. *Inorg. Chem.* **2008**, *47*, 1787–1802.

10.1021/ic900057y CCC: $40.75
Published on Web 04/27/2009

electronic structure theory studies. However, even in monomeric Ru complexes, the assignment of the oxidation state of Ru and the quinone ligand is subject to disagreement for the aqua and hydroxyl species. In fact, in many cases, the assignment of oxidation states of Ru complexes containing quinone ligands has been ambiguous even using data such as X-ray structures, UV-vis, X-ray photoelectron, and EPR spectra.[7−17] Even a detailed analysis of DFT-calculated structures, spin densities, and **g**-tensor anisotropies led to ambiguous (i.e., intermediate) assignments for a series of $[Ru(Q)(acac)_2]^{-,0,+}$ complexes with different Q.[18] Therefore, to fully understand the complicated electronic structures (i.e., metal and quinone oxidation states, and spin multiplicities), and the uniqueness and effectiveness of this dinuclear species as a water oxidation catalyst, we have carried out detailed electronic structure calculations of its related mononuclear species in the gas phase and in aqueous solution with DFT and complete active space self-consistent field (CASSCF) methods, and compare them to results from new, improved electrochemical experiments.

We denote as the "Tanaka monomer" the complex $[Ru(OH_2)(Bu_2Q)(tpy)](ClO_4)_2$ (Bu_2Q = 3,5-di-*tert*-butyl-2,2-benzoquinone, tpy = 2,2′:6′,2″-terpyridine) prepared by Kobayashi et al., who characterized it using various spectroscopic methods to demonstrate the existence of an oxyl radical upon the sequential deprotonation of the water molecule bound to the Ru center.[19] The oxyl radical is believed to be the key species responsible for the catalytic activity of the dimeric species. However, the formal oxidation state assignments for each individual redox couple based upon the experimental measurements are somewhat controversial. A Pourbaix diagram reported by Muckerman et al., based on measured pK_a values of the monomeric species, square-wave voltammograms, and pulse radiolysis studies at various pH provided insights into understanding the coupling between the quinone ligand and the Ru center.[6] The pK_a values of $[Ru(OH_2)(Q)(tpy)]^{2+}$ and $[Ru(OH)(Q)(tpy)]^{1+}$ were determined to be 5.5 and 10.7, respectively, however, the reduction or oxidation of $[Ru(OH_2)(Q)(tpy)]^{2+}$ and related complexes coupled to the deprotonation processes were not fully investigated.

In the present study, we report the results of electronic structure calculations on various intermediate complexes of Tanaka's monomer in the gas phase and aqueous solution. A theoretical Pourbaix diagram is reported to compare with a revised and expanded version of the earlier experimental diagram. Particular focus is given to the possible important role played by the oxyl radical. An expanded interpretation of the Pourbaix diagram based upon theory and new experiments is discussed.

Experimental Section

Syntheses. The complex $[Ru^{II}(OH_2)(Q)(tpy)](ClO_4)_2$ (i.e., $[Ru(OH_2)(Q)]^{2+}$) was prepared as previously described for $[Ru^{III}(OH_2)(SQ)(tpy)](ClO_4)_2$ and characterized by NMR, UV-vis and IR spectroscopy.[19] This complex was originally assigned as $[Ru^{III}(OH_2)(SQ)]^{2+}$ (we will henceforth omit tpy and even Q unless required for clarity) based on XPS data,[19] but we now believe this should be assigned as $[Ru^{II}(OH_2)(Q)]^{2+}$.[6]

Instrumental Measurements. UV-vis spectra were measured on a Hewlett-Packard 8452A diode array spectrophotometer and a Cary 500 Scan UV-vis-NIR spectrophotometer. Square-wave voltammograms were obtained using a BAS100 electrochemical system. Measurements were carried out using only one direction (from the rest potential to positive or negative voltage) in an Ar-filled glovebox or after bubbling Ar that has been passed through a trifluoroethanol/H_2O mixture (v/v 0.02) in a fume hood. The solutions used for the $[Ru(OH_2)(Q)]^{2+}$ experiments contained trifluoroethanol (1−2% by volume) to increase the solubility of $[Ru(OH_2)(Q)]^{2+}$. Between pH 3 and 10, solutions containing 0.01 M phosphate buffer and 0.1 M sodium triflate were used. Between pH 1 and 3, solutions containing 0.1 M triflic acid were used after adjusting the pH with NaOH. Between pH 10 and 12, solutions containing 0.1 M sodium triflate are also used after adjusting the pH with NaOH. Glassy carbon (3 mm diameter), Pt wire and Ag/AgCl (3 M aq. KCl) were used as working, counter and reference electrodes, respectively, in a one-compartment cell. The surface of the working electrode was cleaned by polishing with alumina after each run. An experimental Pourbaix diagram of the Tanaka monomer based on all the new data is shown in Figure 1 along with $E_{1/2}$ lines and oxidation-state and spin-state assignments either corroborated or predicted by the present theoretical results.

Pulse radiolysis studies were carried out using the BNL 2 MeV van de Graaff accelerator with electron pulses (pulse width of 40−500 ns) that led to irradiation doses of 100−1000 rad (ca. 0.5−5 μM primary radicals) generated in solution. A thiocyanate solution (0.01 M KSCN, 0.026 M N_2O) was used for dosimetry taking $G_{(SCN)_2^-} = 6.13$ (G = number of species formed per 100 eV of energy absorbed by the solution) and $\epsilon_{472nm} = (7590 \pm 230)$ $M^{-1}cm^{-1}$. The optical path of the cell was 2 cm.

Radiolysis of aqueous solutions produces •OH, e_{aq}^-, and H• with G values of 2.7, 2.6, and 0.6, respectively ($H_2O \sim\!\!\!\!\!\!\wedge\!\!\!\!\!\!\vee \rightarrow OH^\bullet, e_{aq}^-, H^\bullet, H_2, H_2O_2$).[20] In nitrous-oxide-saturated solution the hydrated electron is converted to OH• ($e_{aq}^- + N_2O + H_2O \rightarrow OH^\bullet + OH^- + N_2$). Radiolysis of a nitrous-oxide-saturated aqueous solution containing HCO_2^- leads to exclusive production of the carbon dioxide anion radical $CO_2^{\bullet-}$, since both OH• and H• react with

(7) Haga, M.; Isobe, K.; Boone, S. R.; Pierpont, C. G. *Inorg. Chem.* **1990**, *29*, 3795–3799.
(8) Pierpont, C. G.; Buchanan, R. M. *Coord. Chem. Rev.* **1981**, *38*, 45–87.
(9) Pierpont, C. G.; Lange, C. W., *Prog. Inorg. Chem.* Wiley: New York, 1993; Vol. 41.
(10) Auburn, P. R.; Dodsworth, E. S.; Haga, M.; Liu, W.; Nevin, W. A.; Lever, A. B. P. *Inorg. Chem.* **1991**, *30*, 3502–3512.
(11) Lever, A. B. P.; Auburn, P. R.; Dodsworth, E. S.; Haga, M.; Wei, L.; Melnik, M.; Nevin, W. A. *J. Am. Chem. Soc.* **1988**, *110*, 8076–8084.
(12) Haga, M.; Dodsworth, E. S.; Lever, A. B. P.; Boone, S. R.; Pierpont, C. G. *J. Am. Chem. Soc.* **1986**, *108*, 7413–7414.
(13) Haga, M.; Dodsworth, E. S.; Lever, A. B. P. *Inorg. Chem.* **1986**, *25*, 447–453.
(14) Bhattacharya, S.; Boone, S. R.; Fox, G. A.; Pierpont, C. G. *J. Am. Chem. Soc.* **1990**, *112*, 1088–1096.
(15) Bhattacharya, S.; Pierpont, C. G. *Inorg. Chem.* **1992**, *31*, 35–39.
(16) Masui, H.; Lever, A. B. P.; Aubrun, P. A. *Inorg. Chem.* **1991**, *30*, 2402–2410.
(17) Kalinina, D.; Dares, C.; Kaluarachchi, H.; Potvin, P. G.; Lever, A. B. P. *Inorg. Chem.* **2008**, *47*, 10110–10126.
(18) Remenyi, C.; Kaupp, M. *J. Am. Chem. Soc.* **2005**, *127*, 11399–11413.
(19) Kobayashi, K.; Ohtsu, H.; Wada, T.; Kato, T.; Tanaka, K. *J. Am. Chem. Soc.* **2003**, *125*, 6729.
(20) Buxton, G. V.; Greenstock, C. L.; Helman, W. P.; Ross, A. B. *J. Phys. Chem. Ref. Data* **1988**, *17*, 513–886.

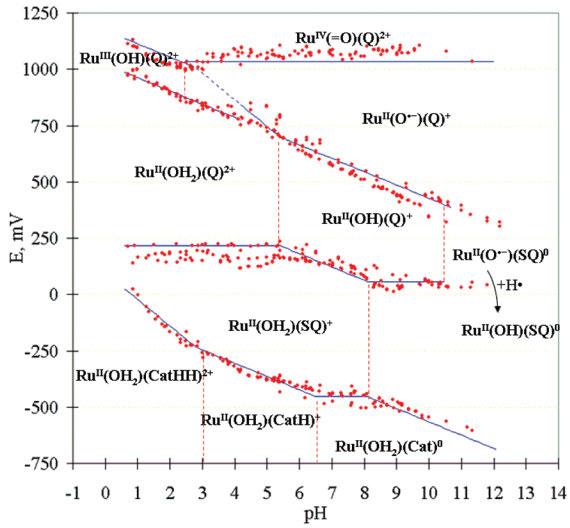

Figure 1. Experimental Pourbaix diagram of $Ru(OH_2)(Q)(tpy)^{2+}$. $E_{1/2}$ is relative to the SCE. CatH (or CatHH) indicates that one (or two) oxygen atom(s) of Cat is (are) protonated.

HCO_2^- ($OH^•/H^• + HCO_2^- \rightarrow H_2O/H_2 + CO_2^{•-}$). $CO_2^{•-}$ is a strong reducing agent ($E = -1.90$ V)[21] that undergoes protonation only under very acidic conditions ($pK_a = -0.2$).[22] An oxidizing radical $(SCN)_2^{•-}$ can be generated by the reaction of potassium thiocyanate with $OH^•$ ($OH^• + SCN^- \rightarrow SCN^• + OH^-$; $SCN^• + SCN^- \rightarrow (SCN)_2^{•-}$).[23] The redox potential of $(SCN)_2^{•-}$ is 1.31 V vs. NHE.[24]

Computational Details. Most calculations were carried out at the density functional theory (DFT) level of theory with the B3LYP functional[25−27] as implemented in the Gaussian 03 program package.[28] The LANL2DZ basis set was used for Ru and all other atoms.[29−32] A vibrational frequency analysis was carried out in order to confirm the minimum geometry and determine the thermal correction, i.e., zero-point energy (ZPE), translational/rotational/vibrational energies, and entropy, of each species under the perfect gas, rigid rotor, and harmonic oscillator approximations. The Mulliken atomic charge and spin populations were also calculated at the optimized geometry. Time-dependent density functional theory (TD-DFT, more specifically TD-B3LYP) was used to validate the ground-state spin multiplicity assignment by computing the first excitation energy.[33−35] Broken-symmetry (BS) calculations were carried out with the Gaussian 03 program following the procedures described elsewhere.[36] To summarize briefly for the case of two unpaired electrons, the alpha- and beta-spin orbitals of the two singly occupied molecular orbitals (SOMOs) resulting from a triplet calculation (with $M_S = 1$) are localized using "guess = mix" if they are not already localized (in which case one uses "guess = alpha"). Then an $M_S = 0$ initial guess is generated by flipping the spin of the alpha electron in the higher-energy localized SOMO of the triplet wave function and moving it to the beta-spin orbital of the lower-energy localized SOMO. An open-shell singlet (OSS) state is obtained by a new SCF calculation in which the spin multiplicity is declared as 1. We have applied this procedure to the calculation of BS states of the main intermediates, i.e., $Ru(OH_2)^{2+}$, $Ru(OH)^+$, and $Ru(O)^0$ (where the Q, SQ, or Cat designation is omitted from the notation due to possible variations) at the lowest-energy geometry of a B3LYP spin-restricted singlet or a spin-unrestricted triplet state. In addition, CASSCF[37−42] calculations at the B3LYP-optimized geometries were carried out to characterize the $Ru(OH_2)^{2+}$, $Ru(OH)^+$, and $Ru(O)^0$ complexes in singlet and triplet states for comparison with the DFT results.

The solvation energy is described by the conductor-like screening model (COSMO),[43] a continuum solvation method appropriate for solvents with high permittivity such as water, at the B3LYP/LANL2DZ level as implemented in Gaussian 03 using the keyword CPCM.[44,45] The molecular cavity was constructed using the united topological model applied with radii optimized for density functional theory denoted as UAKS. Water was used as the solvent in the calculation as represented by dielectric constant $\varepsilon = 78.39$. Only 10 iterations of geometry optimization were carried out in the solvation calculations owing to the slowness of convergence. The lowest energy attained in the 10 iterations, including all nonelectrostatic contributions, was used as the energy minimum.

Additional gas-phase, all-electron B3LYP calculations were carried out using the Orca program[46] and the SV(P) basis[47,48] to exploit the implementation of orbital localization and the identification of corresponding orbitals in the context of BS calculations in that program.

(21) Schwarz, H. A.; Dodson, R. W. *J. Phys. Chem.* **1989**, *93*, 409–414.
(22) Kawanishi, Y.; Kitamura, N.; Tazuke, S. *Inorg. Chem.* **1989**, *28*, 2968–2975.
(23) Adams, G. E.; Boag, J. W.; Currant, J.; Michael, B. D. *In Pulse Raidolysis*; Academic Press: New York, 1965; p 117.
(24) Schwarz, H. A.; Bielski, B. H. J. *J. Phys. Chem.* **1986**, *90*, 1445.
(25) Becke, A. D. *Phys. Rev. A* **1988**, *38*, 3098.
(26) Lee, C.; Yang, W.; Parr, R. G. *Phys. Rev. B* **1988**, *37*, 785.
(27) Miehlich, B.; Savin, A.; Stoll, H.; Preuss, H. *Chem. Phys. Lett.* **1989**, *157*, 200.
(28) Frisch, M. J.; Trucks, G. W.; Schlegel, H. B.; Scuseria, G. E.; Robb, M. A.; Cheeseman, J. R.; Montgomery, J. A., Jr.; Vreven, T.; Kudin, K. N.; Burant, J. C.; Millam, J. M.; Iyengar, S. S.; Tomasi, J.; Barone, V.; Mennucci, B.; Cossi, M.; Scalmani, G.; Rega, N.; Petersson, G. A.; Nakatsuji, H.; Hada, M.; Ehara, M.; Toyota, K.; Fukuda, R.; Hasegawa, J.; Ishida, M.; Nakajima, T.; Honda, Y.; Kitao, O.; Nakai, H.; Klene, M.; Li, X.; Knox, J. E.; Hratchian, H. P.; Cross, J. B.; Bakken, V.; Adamo, C.; Jaramillo, J.; Gomperts, R.; Stratmann, R. E.; Yazyev, O.; Austin, A. J.; Cammi, R.; Pomelli, C.; Ochterski, J. W.; Ayala, P. Y.; Morokuma, K.; Voth, G. A.; Salvador, P.; Dannenberg, J. J.; Zakrzewski, V. G.; Dapprich, S.; Daniels, A. D.; Strain, M. C.; Farkas, O.; Malick, D. K.; Rabuck, A. D.; Raghavachari, K.; Foresman, J. B.; Ortiz, J. V.; Cui, Q.; Baboul, A. G.; Clifford, S.; Cioslowski, J.; Stefanov, B. B.; Liu, G.; Liashenko, A.; Piskorz, P.; Komaromi, I.; Martin, R. L.; Fox, D. J.; Keith, T.; Al-Laham, M. A.; Peng, C. Y.; Nanayakkara, A.; Challacombe, M.; Gill, P. M. W.; Johnson, B.; Chen, W.; Wong, M. W.; Gonzalez, C.; Pople, J. A. *Gaussian 03*, D.01; Gaussian, Inc.: Wallingford, CT, 2004.
(29) Hay, P. J.; Wadt, W. R. *J. Chem. Phys.* **1985**, *82*, 270.
(30) Hay, P. J.; Wadt, W. R. *J. Chem. Phys.* **1985**, *82*, 299.
(31) Wadt, W. R.; Hay, P. J. *J. Chem. Phys.* **1985**, *82*, 284.
(32) Dunning, T. H. J.; Hay, P. J. *Modern Theoretical Chemistry*; Plenum: New York, 1976.
(33) Stratmann, R. E.; Scuseria, G. E.; Frisch, M. J *J. Chem. Phys.* **1998**, *109*, 8218.
(34) Bauernschmitt, R.; Ahlrichs, R. *Chem. Phys. Lett.* **1996**, *256*, 454.
(35) Casida, M. E.; Jamorski, C.; Casida, K. C.; Salahub, D. R. *J. Chem. Phys.* **1998**, *108*, 4439.
(36) Gaussian News, G03 Tips and Techniques, Predicting Antiferromagnetic Coupling, Spring, 2005. http://www.gaussian.com/g_news/sum05/newsletter_g03_tips.htm.
(37) Hegarty, D.; Robb, M. A. *Mol. Phys.* **1979**, *38*, 1795.
(38) Eade, R. H. E.; Robb, M. A. *Chem. Phys. Lett.* **1981**, *83*, 362.
(39) Schlegel, H. B.; Robb, M. A. *Chem. Phys. Lett.* **1982**, *93*, 43.
(40) Bernardi, F.; Bottini, A.; McDougall, J. J. W.; Robb, M. A.; Schlegel, H. B. *Faraday Symp. Chem. Soc.* **1984**, *19*, 137.
(41) Yamamoto, N.; Vreven, T.; Robb, M. A.; Frisch, M. J.; Schlegel, H. B. *Chem. Phys. Lett.* **1996**, *250*, 373.
(42) Frisch, M. J.; Ragazos, I. N.; Robb, M. A.; Schlegel, H. B. *Chem. Phys. Lett.* **1992**, *189*, 524.
(43) Klamt, A.; Schüürmann, G. *J. Chem. Soc., Perkin Trans. 2* **1993**, *799*, 805.
(44) Barone, V.; Cossi, M. *J. Phys. Chem. A* **1998**, *102*, 1995.
(45) Cossi, M.; Rega, N.; Scalmani, G.; Barone, V. *J. Comput. Chem.* **2003**, *24*, 669.
(46) Neese, F. *ORCA, 2.6.63*; Universität Bonn: Bonn, Germany, 2007.
(47) Schäfer, A.; Horn, H.; Ahlrichs, R. *J. Chem. Phys.* **1992**, *97*, 2571.
(48) Ahlrichs, R.; May, K. *Phys. Chem. Chem. Phys.* **2000**, *2*, 943–945.

The pK_a values of various intermediate complexes were calculated in order to compare to the experimental values and to provide data for the construction of a theoretical Pourbaix diagram. The pK_a is defined as

$$pK_a = \Delta G^*_{aq}/2.303RT$$

where R is the universal gas constant and T is the temperature. Here ΔG^*_{aq} is the free energy change for the acid dissociation reaction, $HA_{aq} \rightarrow A^-_{aq} + H^+_{aq}$, at 1 M standard state (the superscript * indicates the standard state of 1 M in both the gas phase and in solution) and can be calculated using a thermodynamic cycle. The ΔG^*_{aq} can be represented as

$$\Delta G^*_{aq} = \Delta G^o_g + \Delta\Delta G^*_s + \Delta G^{o\rightarrow *}$$

where $\Delta G^o_g = G^o_g(A^-) + G^o_g(H^+) - G^o_g(HA)$ and $\Delta\Delta G^*_s = \Delta G^*_s(A^-) + \Delta G^*_s(H^+) - \Delta G^*_s(HA)$. The ΔG^o_g is calculated by ab initio or density functional theory at 1 atm standard state, and ΔG^*_s, the free energy of solvation, is approximated using the COSMO solvation model in the current study. The free energy of the gas-phase proton, $G^o_g(H^+)$, at 298.15 K (−6.28 kcal/mol) was derived from the Sackur−Tetrode equation.[49] The free energy of solvation of the proton, $\Delta G^*_s(H^+)$, at 298 K (−265.87 kcal/mol) reported by Tissandier et al. was also used.[50] Here $\Delta G^{o\rightarrow *}$ is the free energy associated with the difference between the standard states of the gas phase and the aqueous phase (1.89 kcal/mol).

The detailed procedure for calculating pK_a and choosing the values of $G^o_g(H^+)$ and $\Delta G^*_s(H^+)$ has been thoroughly discussed in the literature.[51−101] It should be noted that the ΔG^*_s values reported in the current study do not account for differences in the thermal correction between the gas phase and aqueous phase owing to the difficulty of converging the geometry optimizations in the aqueous phase, i.e., no vibrational frequency analysis was carried out with the continuum solvation model. It is expected that the difference in the thermal correction between the gas and aqueous phases for each intermediate complex will be quite small because no significant geometric change was observed during the first 10 geometry optimization iterations in solution. As a result, the changes in thermal corrections owing to solvation are assumed to cancel in the $\Delta\Delta G^*_s$ term.

The standard reduction potential in aqueous solution was calculated using an approach similar to that described above. The reduction reaction can be expressed by the thermodynamic cycle in which **R** is the reduced acidic species and **O** is the oxidized basic species as shown in Scheme 1. The free energy of the electron in the gas phase is −0.006 kcal/mol.[102] If $m > 0$, the reduction reaction is coupled with proton transfer and denoted as a proton-coupled electron-transfer (PCET) process. The total free energy change in the aqueous phase is obtained from the thermodynamic cycle shown in Scheme 1.

(49) MacQuarrie, D. M. *Statistical Mechanics*; Harper and Row: New York, 1970.
(50) Tissandier, M. D.; Cowen, K. A.; Feng, W. Y.; Gundlach, E.; Cohen, M. H.; Earhart, A. D.; Coe, J. V.; Tuttle, T. R. *J. Phys. Chem. A* **1998**, *102*, 7787.
(51) Schüürman, G.; Cossi, M.; Barone, V.; Tomasi, J. *J. Phys. Chem. A* **1998**, *102*, 6706.
(52) da Silva, C. O.; da Silva, E. C.; Nascimento, M. A. C. *J. Phys. Chem. A* **1999**, *103*, 11194.
(53) Vogel, H. J.; Juffer, A. H. *Theor. Chem. Acc.* **1999**, *101*, 159.
(54) Chen, I.-J.; MacKerell, A. D., Jr. *Theor. Chem. Acc.* **2000**, *103*, 483.
(55) da Silva, C. O.; da Silva, E. C.; Nascimento, M. A. C. *J. Phys. Chem. A* **2000**, *104*, 2402.
(56) Topol, I. A.; Tawa, G. J.; Caldwell, R. A.; Eissenstat, M. A.; Burt, S. K. *J. Phys. Chem. A* **2000**, *104*, 9619.
(57) Jang, Y. H.; Sowers, L. C.; Çagin, T.; Goddard, W. A., III *J. Phys. Chem. A* **2001**, *105*, 274.
(58) Liptak, M. D.; Shields, G. C. *Int. J. Quantum Chem.* **200185**, 727.
(59) Liptak, M. D.; Shields, G. C. *J. Am. Chem. Soc.* **2001**, *123*, 7314–7319.
(60) Ohno, K.; Kamiya, N.; Asakawa, N.; Inoue, Y.; Sakurai, M. *Chem. Phys. Lett.* **2001**, *341*, 387.
(61) Toth, A. M.; Liptak, M. D.; Phillips, D. L.; Shields, G. C. *J. Chem. Phys.* **2001**, *114*, 4595.
(62) Adam, K. *J. Phys. Chem. A* **2002**, *106*, 11963.
(63) Chipman, D. M. *J. Phys. Chem. A* **2002**, *106*, 7413.
(64) Davies, J. E.; Doltsinis, N. L.; Kirby, A. J.; Roussev, C. D.; Sprik, M. *J. Am. Chem. Soc.* **2002**, *124*, 6594.
(65) Feierberg, I.; Åqvist, J. *Theor. Chem. Acc.* **2002**, *108*, 71.
(66) Klicić, J. J.; Friesner, R. A.; Liu, S.-Y.; Guida, W. C. *J. Phys. Chem. A* **2002**, *106*, 1327.
(67) Li, H.; Hains, A. W.; Everts, J. E.; Robertson, A. D.; Jensen, J. H. *J. Phys. Chem. B* **2002**, *106*, 3486.
(68) Liptak, M. D.; Gross, K. C.; Seybold, P. G.; Feldgus, S.; Shields, G. C. *J. Am. Chem. Soc.* **2002**, *124*, 6421.
(69) Lopez, X.; Schaefer, M.; Dejaegere, A.; Karplus, M. *J. Am. Chem. Soc.* **2002**, *124*, 5010.
(70) Satchell, J. F.; Smith, B. J. *Phys. Chem. Chem. Phys.* **2002**, *4*, 4314.
(71) Jang, Y. H.; Goddard, W. A., III; Noyes, K. T.; Sowers, L. C.; Hwang, S.; Chung, D. S. *J. Phys. Chem. B* **2003**, *107*, 344.
(72) Klamt, A.; Eckers, F.; Diedenhofen, M.; Beck, M. E. *J. Phys. Chem. A* **2003**, *107*, 9380.
(73) Eckers, F.; Klamt, A. *J. Comput. Chem.* **2006**, *27*, 11.
(74) Li, G.; Cui, Q. *J. Phys. Chem. B* **2003**, *107*, 14521.
(75) Mujika, J. I.; Mercero, J. M.; Lopez, X. *J. Phys. Chem. A* **2003**, *107*, 6099.
(76) Almerindo, G. I.; Tondo, D. W.; Pliego, J. R., Jr., *J. Phys. Chem. A* **2004**, *108*, 166.
(77) Barone, V.; Improta, R.; Rega, N. *Theor. Chem. Acc.* **2004**, *111*, 237.
(78) da Silva, C. O.; Barbosa, A. G. H.; da Silva, E. T.; da Silva, E. L.; Nascimento, M. A. C. *Theor. Chem. Acc.* **2004**, *111*, 231.
(79) Fu, Y.; Liu, L.; Li, R.-Q.; Liu, R.; Guo, Q.-X. *J. Am. Chem. Soc.* **2004**, *126*, 814.
(80) Namazian, M.; Halvani, S.; Noorbala, M. R. *J. Mol. Struct.: THEOCHEM* **2004**, *711*, 13.
(81) Quenneville, J.; Popovic, D. M.; Stuchebrukhov, A. A. *J. Phys. Chem. B* **2004**, *108*, 18383.
(82) Schmidt am Busch, M.; Knapp, E. W. *ChemPhysChem* **2004**, *5*, 1513.
(83) Simonson, T.; Carlsson, J.; Case, D. A. *J. Am. Chem. Soc.* **2004**, *126*, 4167.
(84) Curutchet, C.; Bidon-Chanal, A.; Soteras, I.; Orozco, M.; Luque, F. J. *J. Phys. Chem. B* **2005**, *109*, 3565.
(85) Han, J.; Deming, R. L.; Tao, F.-M. *J. Phys. Chem. A* **2005**, *109*, 1159.
(86) Jensen, J. H.; Li, H.; Robertson, A. D.; Molina, P. A. *J. Phys. Chem. A* **2005**, *109*, 6634.
(87) Kaminski, G. A. *J. Phys. Chem. B* **2005**, *109*, 5884.
(88) Popovic, D. M.; Quenneville, J.; Stuchebrukhov, A. A. *J. Phys. Chem. B* **2005**, *109*, 3616.
(89) Takano, Y.; Houk, K. N. *J. Chem. Theory Comput.* **2005**, *1*, 70.
(90) Wang, X.; Li, S.; Jang, Y. *J. Phys. Chem. A* **2005**, *109*, 10776.
(91) Gao, D.; Sovronos, P.; Wong, P. K.; Maddalena, D.; Hwang, J.; Walker, H. J. *J. Phys. Chem. A* **2005**, *109*, 10776.
(92) Kelly, C. P.; Cramer, C. J.; Truhlar, D. G. *J. Phys. Chem. A* **2006**, *110*, 2493.
(93) Kelly, C. P.; Cramer, C. J.; Truhlar, D. G. *J. Phys. Chem. B* **2006**, *110*, 16066.
(94) Krol, M.; Wrona, M.; Page, C. S.; Bates, P. A. *J. Chem. Theory Comput.* **2006**, *2*, 1520.
(95) Kelly, C. P.; Cramer, C. J.; Truhlar, D. G. *J. Phys. Chem. B* **2007**, *111*, 408.
(96) Yu, A.; Liu, Y. H.; Wang, Y. J. *Chem. Phys. Lett.* **2007**, *436*, 276.
(97) Bryantsev, V. S.; Diallo, M. S.; Goddard, W. A., III *J. Phys. Chem. A* **2007**, *111*, 4422.
(98) Jia, Z. K.; Du, D. M.; Zhou, Z. Y.; Zhang, A. G.; Hou, R. Y. *Chem. Phys. Lett.* **2007**, *439*, 374.
(99) Sadlej-Sosnowska, N. *Theor. Chem. Acc.* **2007**, *118*, 281.
(100) Marenich, A. V.; Olson, R. M.; Kelly, C. P.; Cramer, C. J.; Truhlar, D. G. *J. Chem. Theory Comput.* **2007**, *3*, 2011.
(101) Jia, Z. K.; Mang, S. F.; Zhou, Z. Y.; Mang, A. G.; Hou, R. Y. *Int. J. Quantum Chem.* **2008**, *108*, 265.
(102) Lewis, A.; Bumpus, J. A.; Truhlar, D. G.; Cramer, C. J. *J. Chem. Educ.* **2004**, *81*, 596–604.

The $G_g^o(H^+)$, $\Delta G_s^*(H^+)$, and $\Delta G^{o\rightarrow *}$ in Scheme 1 have the same values as indicated above. The standard reduction potential can be described by the following equation:

$$E^*_{O|R} = -\frac{\Delta G^*_0}{nF} - E^*_{SCE} = -\frac{(\Delta G^*_{O|R} - n\cdot\Delta G^*_{NHE})}{nF} - E^*_{SCE}$$

where ΔG_0^* is the standard free energy change relative to the normal hydrogen electrode (NHE) and ΔG^*_{NHE} was reported as 4.28 eV. The standard reduction potential reported in the current study is shifted by −0.24 V with respect to the NHE because of the standard reference electrode (E^*_{SCE} = +0.24 V vs NHE) used in the experiments. The details of calculating the standard reduction potential have been well documented in the literature.[103−129] In the case of $m > 0$, the standard reduction potential of the PCET is calculated at pH 0. The pH-dependent reduction potential is specified by the Nernst Equation:

$$E = E^*_{O|R} + \frac{RT}{nF}\ln\left(\frac{a_O}{a_R}\right) - \frac{m}{n}\cdot 0.0591\cdot \mathrm{pH}$$

where m and n denote the number of protons and electrons, respectively, R is universal gas constant, T is the temperature, F is the Faraday constant, and a_i is the chemical activity of species i (i = O or R). At the half-potential for the reduction reaction, the second term is equal to zero.

Scheme 1. Thermodynamic Cycle for the Standard Free Energy of Reaction for the Proton-Coupled Reduction of Species O to Species R in the Gas Phase and in Aqueous Solution

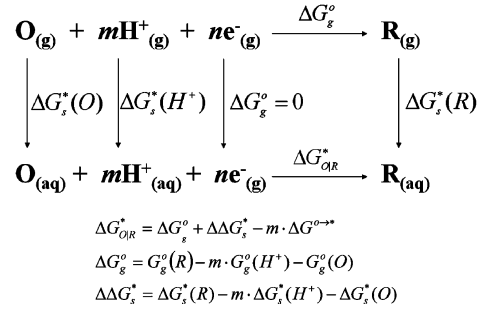

It should be noted that the predicted pK_a and standard reduction potential can vary owing to the convergence of the solvation energy calculation and limitations of the solvation model. The "theoretical precision" of the solvation energy is expected to be 2−3 kcal/mol and that can be translated to 2 pK_a units and 130 mV. The true error in the calculation of solvation energy differences is probably larger than that for gas-phase free energy differences arising from basis set deficiencies.

Results

Singlet States, Triplet States, Broken Symmetry States, and Beyond. The correct identification of the ground states is important both for the assignment of formal oxidation states of redox couples and for calculating pK_a values and standard reduction potentials of the various species of the Tanaka catalyst monomer. Density functional theory is the tool of choice for the latter of these considerations because of its treatment of electron correlation through the correlation functional. The DFT treatment of electron correlation, however, is not completely satisfactory in some cases.

Because of the multiple redox couples in the species under consideration, it is not surprising that singlet and triplet states can have similar energies, and effects beyond the single-configuration approximation can sometimes determine the true ground electronic state. Qualitative insight into such cases can often be gained by small CASSCF calculations that introduce specific valence configuration interaction (CI) into the electronic wave function, but such calculations are not quantitatively accurate because of their neglect of other electron correlation. Here we briefly discuss how we deal with this problem and how we interpret a broken-symmetry result.

We calculate both the singlet, closed-shell and broken-symmetry (BS),[130,131] and triplet B3LYP energies of a given species along with supplemental CASSCF calculations. If the BS energy is lower than the triplet energy, the interaction between the two spins is designated as "antiferromagnetic coupling," otherwise it is "ferromagnetic coupling." If the BS solution has not collapsed to the closed-shell-singlet state (i.e., the alpha- and beta-spin HOMO orbitals become identical and $<S^2> = 0$), this implies a singlet biradical (i.e.,

(103) Winget, P.; Weber, E. J.; Cramer, C. J.; Truhlar, D. G. *Phys. Chem. Chem. Phys.* **2000**, *2*, 1231.
(104) Winget, P.; Cramer, C. J.; Truhlar, D. G. *Theor. Chem. Acc.* **2004**, *112*, 217.
(105) Reynolds, C. A.; King, P. M.; Richards, W. G., *J. Chem. Soc. Chem. Commun.* **1988**, *1434*.
(106) Reynolds, C. A.; King, P. M. ; Richards, W. G., *Nature (London)* **1988**, (*334*).
(107) Lister, S. G.; Reynolds, C. A.; Richards, W. G. *Int. J. Quantum Chem.* **1992**, *41*, 293.
(108) Wolfe, J. J.; Wright, J. D.; Reynolds, C. A.; Saunders, A. C. G. *Anti-Cancer Drug Des.* **1994**, *9*, 85.
(109) Reynolds, C. A. *Int. J. Quantum Chem.* **1995**, *56*, 677.
(110) Boesch, S. E.; Grafton, A. K.; Wheeler, R. A. *J. Phys. Chem.* **1996**, *100*, 10083.
(111) Raymond, K. S.; Grafton, A. K.; Wheeler, R. A. *J. Phys. Chem. B* **1997**, *101*, 623.
(112) Kettle, L. J.; Bates, S. P.; Mount, A. R. *Phys. Chem. Chem. Phys.* **2000**, *2*, 195.
(113) Kaszynski, P. *J. Phys. Chem. A* **2001**, *105*, 7626.
(114) Fabre, B.; Hapiot, P.; Simonet, J. *J. Phys. Chem. A* **2002**, *106*, 5422.
(115) Fontanesi, C.; Benassi, R.; Giovanardi, R.; Marcaccio, M.; Paolucci, F.; Roffia, S. *J. Mol. Struct.* **2002**, *612*, 277.
(116) Baik, M.-H.; Friesner, R. A. *J. Phys. Chem. A* **2002**, *106*, 7407.
(117) Baik, M.-H.; Friesner, R. A.; Ziegler, T. *J. Am. Chem. Soc.* **2002**, *124*, 11167.
(118) Namazian, M.; Norouzi, P.; Ranjbar, R. *J. Mol. Struct.: THEOCHEM* **2003**, *625*, 235.
(119) Namazian, M. *J. Mol. Struct.: THEOCHEM* **2003**, *664*, 273.
(120) Benassi, R.; Ferrarini, P.; Fontanesi, C.; Benedetti, L.; Paolucci, F. *J. Electroanal. Chem.* **2004**, *564*, 231.
(121) Namazian, M.; Almodarresieh, H. A. *J. Mol. Struct.: THEOCHEM* **2004**, *686*, 97.
(122) Fu, Y.; Liu, L.; Yu, H.-Z.; Wang, Y.-M.; Guo, Q.-X. *J. Am. Chem. Soc.* **2005**, *127*, 7227.
(123) Dutton, A. S.; Fukuto, J. M.; Houk, K. N. *Inorg. Chem.* **2005**, *44*, 4024.
(124) Camurri, G.; Ferrarini, P.; Giovanardi, R.; Benassi, R.; Fontanesi, C. *J. Electroanal. Chem.* **2005**, *585*, 181.
(125) Shamsipur, M.; Alizadeh, K.; Arshadi, S. *J. Mol. Struct.: THEOCHEM* **2006**, *758*, 71.
(126) Wass, J. R. T. J.; Ahlberg, E.; Panas, I.; Schiffrin, D. J. *J. Phys. Chem. A* **2006**, *110*, 2005.
(127) Bottoni, A.; Cosimelli, B.; Scavetta, E.; Spinelli, D.; Spisani, R.; Stenta, M.; Tonello, D. *Mol. Phys.* **2006**, *104*, 2961.
(128) Jaque, P.; Marenich, A. V.; Cramer, C. J.; Truhlar, D. G. *J. Phys. Chem. C* **2007**, *111*, 5783.
(129) Bhattacharyya, S.; Stankovich, M. T.; Truhlar, D. G.; Gao, J. L. *J. Phys. Chem. A* **2007**, *111*, 5729.
(130) Neese, F. *J. Phys. Chem. Solids* **2004**, *65*, 781–785.
(131) Noodleman, L. *J. Chem. Phys.* **1981**, *74*, 5737–5743.

open-shell singlet, or OSS) ground state in the localized orbital picture. But how should we interpret cases in which $<S^2>$ is intermediate between 0 and 2, and the BS energy is lower than both the pure singlet and triplet energies?

Supporting Information Figure S1 displays the results of a series of CAS(2,2) calculations, i.e., CASSCF calculations with two active electrons and two active orbitals, corresponding to the dissociation of H_2 by stretching the internuclear distance from its equilibrium value to larger and larger values. These results show that a generalized valence bond (GVB) configuration interaction in which a second configuration with the pair of electrons in the σ_g orbital promoted to the σ_u orbital becomes increasingly important as the bond is stretched. This allows the H_2 molecule to dissociate into two neutral H atoms as the CI coefficients of the σ_g^2 and σ_u^2 configurations approach the same magnitude. There is a small amount (ca. two percent) of σ_u^2 character in the wave function at small internuclear distances, but it only becomes appreciable as the molecule is stretched. The effect of the GVB-CI lowers the energy of the CAS(2,2) curve below the Hartree−Fock (HF) curve, and introduces some singlet biradical character into the wave function. The energy-lowering effect is appreciable even at the minimum, and becomes quite large in the region where we would still identify σ_g^2 as the dominant configuration (i.e., before the percentage of the σ_u^2 configuration approaches 25%). On this basis, we would not identify H_2 as being predominantly a singlet biradical species at internuclear distances smaller than ca. 2 Å although it would have some singlet biradical character.

If we were to describe the same H_2 dissociation process in terms of the BS approach, the wave function would collapse into the closed-shell σ_g^2 configuration near the equilibrium separation, then gradually converge to a more and more localized orbital solution as the molecule is stretched. Correspondingly, $<S^2>$ would gradually increase from 0 to a value near 1 because at infinite separation the singlet and triplet states are degenerate, and the BS wave function becomes an equal mixture of the $M_S = 0$ singlet and triplet wave functions. This is an example of GVB-CI stabilizing the singlet wave function.

There is also, however, the possibility that multiconfigurational effects in the triplet wave function are important enough to produce a triplet ground-state with lower energy than the single-configuration triplet, as we believe is the case in the oxyl radical discussed below. In such a case, flipping the spin in the BS approach to create an $M_S = 0$ wave function can introduce "new" triplet character that was not in the $M_S = 1$ solution (e.g., $M_S = 0$ character of a GVB-CI triplet involving orbitals other than the SOMOs of the $M_S = 1$ triplet), and thereby lower the energy. In such a case, we would expect $<S^2>$ to be significantly larger than 1, and we would not designate such a state as "antiferromagnetic."

Electronic Assignments of Intermediate Complexes. The calculated Mulliken charge and spin populations at the optimized geometries for the various intermediate complexes are reported in Supporting Information Tables S1 and S2. The electronic assignment of their redox states is summarized in Table 1. These indicators provide more insight into the open-shell species than the closed-shell species because the spin-density, which is unique to open-shell species, is a more physically meaningful quantity than the atomic charge in a molecule. There are three main intermediate states for this Ru-containing monomer, i.e., $Ru(OH_2)^{2+}$, $Ru(OH)^{+}$, and $Ru(O)^0$, corresponding to different stages of deprotonation without oxidation. CASSCF molecular orbitals for singlet (S) and triplet (T) states of $Ru(OH_2)^{2+}$, $Ru(OH)^{+}$, and $Ru(O)^0$ at DFT optimized geometries are shown in Figure 2. The electronic state of the singlet $Ru(OH_2)^{2+}$ complex is assigned as $Ru^{II}(OH_2)(Q)(tpy)^{2+}$ based on the calculated Mulliken charge. The calculated charges are 0.698, 0.194, 0.778, 0.330 for Ru, water, terpyridine (tpy), and quinone (Q), respectively. Considering the number of coordination bonds of each ligand, and the charge transfer effect, the charges can be redistributed as 0.194 for Ru—O (of H_2O), 0.259 for Ru—N (of tpy), and 0.165 for Ru—O (of Q). It is seen that the magnitude of the charge transfer effect is roughly equivalent through each coordination bond. By adding the additional constraint of a closed-shell electronic configuration in the calculation, the electronic assignment of singlet $Ru(OH_2)^{2+}$ can only be $Ru^{II}(OH_2)(Q)(tpy)^{2+}$ given the moderate charge transfer effect shown in the calculated Mulliken charge. The triplet state counterpart is assigned as $Ru^{III}(OH_2)(SQ)(tpy)^{2+}$, i.e., one-electron transfer from Ru^{II} to the Q ligand from the singlet state to make a triplet state. The calculated spin density indicates unpaired electrons on Ru and Q, although there were only minor changes in the Mulliken charge distribution compared to the singlet state.

Table 1. Electronic Assignment of the Main Intermediate Complexes and Their Reduced and Oxidized Species[a,b]

	Ru-OH_2	Ru-OH	Ru−O
S	$Ru^{II}(OH_2)(Q)(tpy)^{2+}$	$Ru^{II}(OH)(Q)(tpy)^{+}$	$Ru^{IV}(=O)(Cat)(tpy)^0$
T	$Ru^{III}(OH_2)(SQ)(tpy)^{2+}$	$Ru^{III}(OH)(SQ)(tpy)^{+}$	$Ru^{II}(O^{\bullet-})(SQ)(tpy)^0$
OSS	Converged to S	$Ru^{III}(OH)(SQ)(tpy)^{+}$	$Ru^{II}(O^{\bullet-})(SQ)(tpy)^0$
S(+2e)	$Ru^{II}(OH_2)(Cat)(tpy)^0$	$Ru^{II}(OH)(Cat)(tpy)^{-}$	$Ru^{II}(O)(Cat)(tpy)^{2-}$
T(+2e)	$Ru^{II}(OH_2)(SQ)(tpy^{\bullet-})^0$	$Ru^{I}(OH)(Q)(tpy^{\bullet-})^{-}$	$Ru^{II}(O^{\bullet-})(Cat)(tpy^{\bullet-})^{2-}$
D(+1e)	$Ru^{II}(OH_2)(SQ)(tpy)^{+}$	$Ru^{II}(OH)(SQ)(tpy)^0$	$Ru^{II}(O^{\bullet-})(Cat)(tpy)^{-}$
D(−1e)	$Ru^{III}(OH_2)(Q)(tpy)^{3+}$	$Ru^{III}(OH)(Q)(tpy)^{2+}$	$Ru^{II}(O^{\bullet-})(Q)(tpy)^{+}$
S(−2e)			$Ru^{IV}(=O)(Q)(tpy)^{2+}$
T(−2e)			$Ru^{III}(O^{\bullet-})(Q)(tpy)^{2+}$

[a] S, T, and D denote the singlet, triplet and doublet spin states, respectively, and the parentheses denote the two-electron reduced (+2e), one-electron reduced (+1e), one-electron oxidized (−1e) or two-electron oxidized (−2e) form. [b] It should be noted that the assignment avoids using fractional charge and the spin density is localized on the ligands with the major contribution.

The singlet $Ru(OH)^{+}$ is assigned as $Ru^{II}(OH)(Q)(tpy)^{+}$. The calculated charge on the deprotonated water moiety is −0.214, indicating the existence of OH^{-}. The π donation from OH^{-} increases as H^{+} is abstracted from the water ligand of the $Ru(OH_2)^{2+}$ species, and that tends to partially neutralize the positive charge of Ru^{II}. The calculated Ru—O (of the water moiety) stretching frequency is also in agreement with this interpretation, increasing from 393 cm^{-1} to 578 cm^{-1} as shown in Supporting Information Table S3. The stronger π donation to the metal center results in only a minor change in the charge on Q and tpy. The triplet $Ru(OH)^{+}$ is assigned as $Ru^{III}(OH)(SQ)(tpy)^{+}$ where the unpaired electron density was predicted to be on Ru and Q. This seems reasonable because this complex is more likely

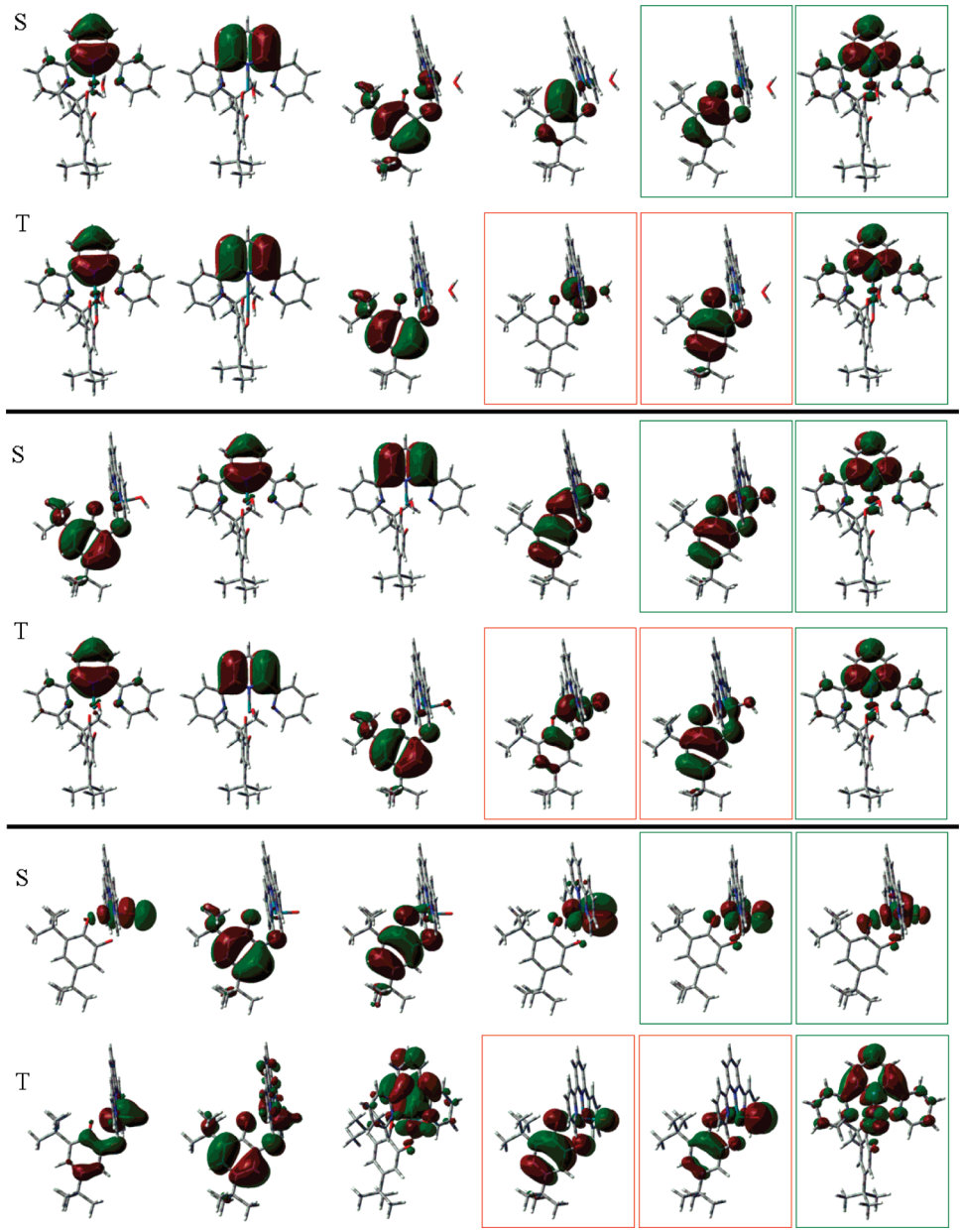

Figure 2. Active space molecular orbitals from CAS(8,6) calculations for singlet (S) and triplet (T) $Ru(OH_2)^{2+}$, rows 1 and 2; $Ru(OH)^{+}$, rows 3 and 4; and $Ru(O)^{0}$, rows 5 and 6 complexes, respectively, at DFT optimized geometries. The red boxes denote singly occupied MOs and the green boxes unoccupied MOs in the principal configurations.

to prefer to be Ru^{III}, OH^{-} and SQ than Ru^{II}, $OH^{\bullet}$, and SQ. The BS $Ru(OH)^{+}$ is assigned the same as the triplet state but with singlet-coupled ("antiferromagnetically coupled") unpaired spins. This "all-or-nothing" aspect of the BS method, which is still a single-configuration method, cannot adequately describe a predominantly closed-shell singlet with enough singlet biradical character arising from a GVB-CI to produce a singlet ground state, as we believe the correct assignment to be. Nevertheless, we believe the BS energy to be the best available approximation to the true multiconfigurational singlet state energy.

There is strong experimental spectroscopic evidence that the $Ru(OH)^{+}$ species is not an antiferromagnetically coupled state with unpaired spins on Ru^{III} and SQ: In the base titration of $Ru(OH_2)^{2+}$ the species in solution continues to exhibit the spectral signature of the quinone ligand (metal-to-ligand charge transfer (MLCT) band at ca. 600 nm) until more than two equivalents of base have been added. The spectral signature of the semiquinone ligand (peak at ca. 870 nm) appears only when the pH was higher than the second pK_a of $Ru(OH_2)^{2+}$.[19] Furthermore, there is additional experimental evidence of a low-temperature triplet EPR signal from the species produced by rapidly cooling to 4 K a solution of $Ru(OH_2)^{2+}$ after the addition of excess base.[19] It is interesting that the $Ru(OH)^{+}$ complex has not yet been oxidized despite one proton having been abstracted from it. This is consistent with the dihydroxy form of the dimeric Tanaka catalyst that was isolated and characterized as being a diamagnetic species. The O—O bond formation in the dimer may likely occur upon the second deprotonation of both water moieties.

The singlet $Ru(O)^{0}$ is assigned as $Ru^{IV}(=O)(Cat)(tpy)^{0}$ due to the doubly occupied π^* orbital of the quinone ligand and

Table 2. Energetics[a] and Other Properties[b] of Singlet, Triplet, And Open-Shell Singlet States of $Ru(OH_2)^{2+}$ and its Deprotonated Species

	$Ru(OH_2)^{2+}$	$Ru(OH)^{+}$	$Ru(O^{\bullet -})^{0}$
E(S)[a]	−1608.18752	−1607.87327	−1607.40781
E(T)[a]	−1608.17421	−1607.87638	−1607.42306
E(BS)[a]	−1608.18752	−1607.87935	−1607.42425
G(S)[a]	−1607.67996	−1607.37672	−1606.92413
G(T)[a]	−1607.66835	−1607.38261	−1606.94316
G(BS)[a]		−1607.38331	−1606.94184
ΔG_{sol}(S)[b]	−108.45	−22.04	−6.99
ΔG_{sol}(T)[b]	−111.85	−22.99	−4.81
ΔG_{sol}(BS)[b]		−22.29	−1.40
CAS(8,6)[c]			
E_{CAS}(S)[c]	−1597.70346	−1597.35508	−1596.89300
Config(S)[c]	91%(222200):6%(222020)	69%(222200):28%(222020)	87%(222200):9%(222020)
E_{CAS}(T)[c]	−1597.66914	−1597.34813	−1596.85497
Config(T)[c]	97%(222110):2%	97%(222110):3%	85%(222110):14%(220112)
ORCA[d]			
E(S)[a]	−5955.499359	−5955.187292	−5954.716733
E(T)[a]	−5955.476136	−5955.187997	−5954.735471
E(BS)[a]	−5955.499362	−5955.192357	−5954.736795
$<S^2>_T$	2.009	2.014	2.478
$<S^2>_{BS\text{-}ini}$	0.003	0.866	1.368
$<S^2>_{BS\text{-}opt}$	0.000	0.712	1.393

[a] Electronic energies are in atomic units (a.u.). [b] Solvation energies are in kcal/mol. [c] CASSCF(8,6) calculations were carried out at DFT optimized geometries. The percentage of the two most dominant configurations is reported with the occupation numbers of the active space orbitals listed in the parentheses. [d] B3LYP energies and expectation values of S^2 for singlet, triplet and broken symmetry calculations with the all-electron SV(P) basis using the Orca program.

the unoccupied Ru(O) π^* orbital (i.e., any "antiferromagnetically coupled" $Ru^{III}(O^{\bullet -})$ character must arise from a GVB-CI from the Ru(O) π orbital to the Ru(O) π^* orbital, and we will see that this latter configuration accounts for only 9% of the CAS(8,6) wave function) as shown in the fifth row of Figure 2. There is also much more negative charge on Q compared to singlet $Ru^{II}(OH)(Q)(tpy)^{+}$. The calculated Ru−O (of the water moiety) stretching frequency is significantly blue-shifted to 784 cm^{-1} as shown in Supporting Information Table S3 and suggests the existence of Ru═O character. There is yet additional evidence supporting the assignment of Cat. The C4−C5 distance decreases from 1.472 Å in singlet $Ru^{II}(OH_2)(Q)(tpy)^{2+}$ to 1.433 Å in the calculated singlet state of $Ru(O)^0$, whereas the mean C3−C4 and C5−C6 distance increases from 1.387 to 1.401 Å. Further support for this assignment is provided by the carbon−carbon distances of the Cat ligand in the two-electron-reduced form of singlet $Ru^{II}(OH_2)(Q)(tpy)^{2+}$, assigned as $Ru^{II}(OH_2)(CatH)(tpy)^{+}$ at moderate pH, and $Ru^{II}(OH_2)(Cat)(tpy)^0$ at high pH. In the latter, the C4−C5 distance is 1.416 Å and the mean C3−C4 and C5−C6 distance is 1.412 Å.

Despite the DFT calculation of triplet $Ru(O)^0$ being spin-contaminated, the electronic configuration is assigned as $Ru^{II}(O^{\bullet -})(SQ)(tpy)^0$ as also supported by the CAS(8,6) calculation. A TD-DFT calculation predicts the next-lowest triplet electronic configuration, $Ru^{III}(O^{\bullet -})(Cat)(tpy)^0$, to be 2.24 kcal/mol higher than the ground state. Interestingly, a restricted open-shell Hartree−Fock (ROHF) calculation at the DFT optimized geometry predicts $Ru^{III}(O^{\bullet -})(Cat)(tpy)^0$ to be 0.57 kcal/mol higher than $Ru^{II}(O^{\bullet -})(SQ)(tpy)^0$. The CAS(8,6) calculation, which takes into account both configurations, converges to $Ru^{II}(O^{\bullet -})(SQ)(tpy)^0$ (see Figure 2), and the two-state-averaged CAS(8,6) predicts that $Ru^{III}(O^{\bullet -})(Cat)(tpy)^0$ is 14.7 kcal/mol higher. The electronic configuration $Ru^{III}(O^{2-})(SQ)(tpy)^0$ would be still higher in energy because the d_π orbital of the Ru^{III} is singly occupied and cannot accept a donated electron pair from the O^{2-} to form a Ru−O double bond.

The electronic states and their assignments of the two-electron reduced species with or without protonation, the one-electron reduced species, and the one-electron oxidized species of the main intermediate states were also considered. The electronic assignments of these redox states were also partially based upon calculated Mulliken charge and spin populations reported in Supporting Information Tables S1 and S2 and Table 1.

Gas-Phase Energetics. The energetics of all the important Tanaka monomer species at the density functional level of theory are reported in Table 2. For the $Ru(OH_2)^{2+}$ complexes, the free energy of the singlet state relative to the triplet state is −7.29 kcal/mol in the gas phase, whereas the BS OSS state wave function collapses back to a closed-shell owing to strong coupling between Ru and the quinone ligand. The Orca BS B3LYP calculation with the all-electron SV(P) basis converges to the closed-shell singlet ($<S^2> = 0.003$) that is 17.18 kcal/mol below the triplet state. For the $Ru(OH)^{+}$ complexes, the gas-phase free energy of the BS B3LYP OSS state is lower than the singlet and triplet states by 4.14 and 0.44 kcal/mol, respectively. The Orca BS B3LYP calculation with the SV(P) basis gives an antiferromagnetic ground state with $<S^2> = 0.712$. For the $Ru(O)^0$ complexes, the gas-phase free energy of the triplet state is 11.94 and 0.83 lower than the singlet and BS OSS states, respectively, despite the BS OSS being slightly lower than the triplet before taking thermal corrections into account. The Orca BS B3LYP calculation with the SV(P) basis gives an antiferromagnetic ground state with $<S^2> = 1.393$.

Restricted Hartree−Fock (RHF), ROHF, and CASSCF calculations were carried out at the B3LYP-optimized geometries to compare with DFT results. It should be noted that DFT and ROHF calculations predict the same electronic states for all the intermediates, as mentioned above. A series of CAS(2,2) calculations was carried out for all the possible

pairings of a frontier valence orbital and a low-lying virtual orbital from the RHF/ROHF calculation. The orbitals from the lowest-energy CAS(2,2) wave function were then used as the initial guess for a larger CAS(8,6) calculation. The idea underlying the use of CAS(2,2) orbitals as the initial guess is that only one dominant GVB pair or two unpaired electrons is expected for the current system. The initial guess from CAS(2,2) orbitals leads to much faster and correct convergence of the CAS(8,6) wave function in comparison with starting from the HF or ROHF orbitals. This idea can be generalized to larger systems such as the Tanaka's dimer in which up to two GVB pairs or four unpaired electrons might be expected, and thus the orbitals from a CAS(4,4) wave function would be a better initial guess. The (8,6) active space is chosen to include the π and π^* orbitals of quinone, two Ru—O (of aqua) bonding orbitals, and the π and π^* orbitals of tpy for the singlet complexes. The occupied orbitals of this set are separated energetically from the other occupied orbitals.

The CAS(8,6) calculations (see Table 2 and Figure 2) show that all of the singlet-state complexes have multiconfigurational character with 91:6%, 69:28%, and 87:9% contributions from the most and second-most important configurations in the +2, +1, and neutral complexes, respectively. The corresponding triplet states are single-configurational except for the $Ru(O)^0$ triplet where two important configurations are seen with 85:14% contributions. The multiconfigurational character is of a generalized valence bond (GVB) type in which a pair of electrons of the metal—ligand bonding orbital is promoted to the corresponding antibonding orbital (see Figure 2). This multiconfigurational character is not included in the formalism of the single-reference-based density functional theory despite the fitting of the exchange-correlation functional to an experimental data set that may fortuitously account for some of this effect. Although the BS approach predicts an "antiferromagnetic" state with lower energy than the pure-spin DFT states, and better agreement with the multiconfigurational description with respect to enegetics,[131,132] it does not qualitatively identify the same ground state that is predicted by the CASSCF approach. A similar paradox has been observed and reported by Batista and Martin in the case of the Blue Dimer catalyst.[133]

Another important factor affecting the energetics is electron correlation. It is known that the employment of an exchange-correlation functional for explicitly treated electrons (and even some correlation in the effective core potentials) in density functional theory is not a "complete" description. Moreover, the CASSCF calculations only account for electron correlation within the active space. The complete treatment of electron correlation in CASSCF requires using a full CI expansion through the entire molecular orbital space, but that is computationally prohibitive for the current system. The low-lying exited states predicted in the TD-B3LYP calculations, as shown in Supporting Information Table S4, raise concern about using second-order Møller—Plesset perturbation theory (MP2), another conventional method for treating electron correlation. The low-lying excited states, as calculated in B3LYP potential energy surfaces (PESs), are expected to be accessible from the HF and CASSCF PESs and cause the electron correlations to be overestimated in an MP2 treatment. As a consequence, we still reply on the BS-DFT approach for calculating electrochemical properties because that methodology may provide a relatively better zero-order description.

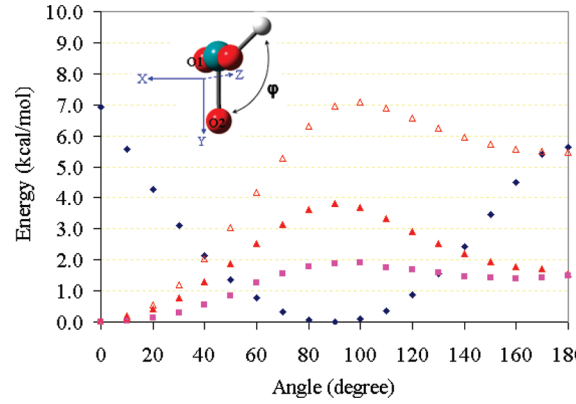

Figure 3. Relative energy scan in kcal/mol of rigid H-O—Ru-O2 dihedral angle rotation of $Ru(OH)^+$: BS state (triangles), $Ru(OH)^{2+}$ doublet state (diamonds), and $Ru(OH)^0$ doublet state (squares). The open and solid symbols denote gas and solution phases, respectively.

Solvation Effects. The gas-phase optimized geometry of $Ru(OH)^+$ is predicted to have a dihedral angle for H-O—Ru-O1 (of the quinone ligand) of 0 degrees with the H of OH located on the same side of the Ru—O axis as the O2 of the quinone ligand. A second "minimum" (one imaginary frequency corresponding to H-O—Ru-O2 dihedral rotation in the gas phase) with a H-O—Ru-O1 dihedral angle of 180 degrees is 5.48 kcal/mol higher than the first, as shown in Figure 3. The calculated dipole moment of the second minimum is 8.1 Debye, whereas that at the first minimum is 4.8 Debye. Fully relaxed solution-phase optimizations (10 iterations) starting near 0 or 180 degrees using a continuum model predict that both the 0- and 180-degree minima have essentially the same energy, less than a 0.05 kcal/mol difference. Upon microsolvating $Ru(OH)^+$ with two explicit water molecules in the gas phase, the dihedral angle of H-O—Ru-O2 at the lowest minimum is calculated to be 154 degrees (not shown). Adding a continuum solvent model to $(H_2O)_2 \cdot Ru(OH)^+$ favors the H-O—Ru-O2 180-degree dihedral angle minimum. Consequently, the H-O—Ru-O2 180-degree minimum, after correcting the zero-point energy (ZPE) for the missing vibration in the gas-phase free-energy calculation, is used in constructing the Pourbaix diagram. The details of the ZPE correction are given in the Supporting Information.

Interestingly, the $Ru(OH)^{2+}$ and $Ru(OH)^0$ species do not favor the 180-degree dihedral angle in solution phase. The oxidized species, $Ru(OH)^{2+}$, has a deep minimum at a H-O—Ru-O2 dihedral angle of 90 degrees as shown in Figure 3. For the reduced species, $Ru(OH)^0$, the calculated dipole moment of the 0-degree minimum is 5.1 Debye, while at the 180-degree minimum it is 6.8 Debye. The dipole moment

(132) Noodleman, L.; Lovell, T.; Han, W.-G.; Li, J.; Himo, F. *Chem. Rev.* **2004**, *104*, 459–508.
(133) Batista, E. R.; Martin, R. L. *J. Am. Chem. Soc.* **2007**, *129*, 7224–7225.

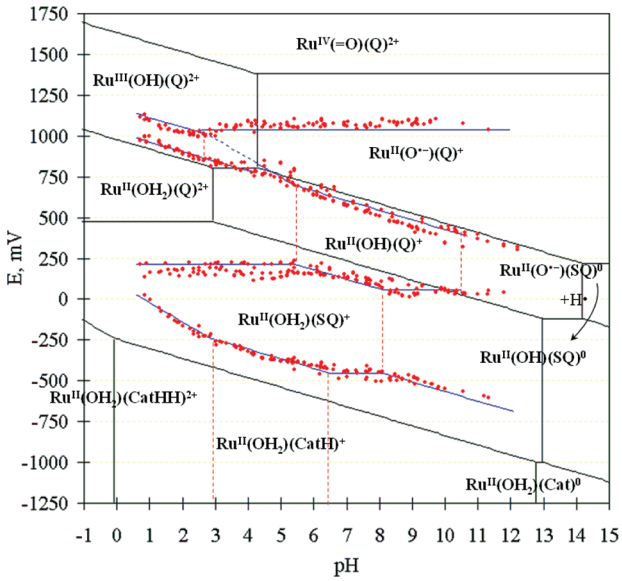

Figure 4. An experimental and theoretical Pourbaix diagram of $Ru(OH_2)(Q)(tpy)^{2+}$. $E_{1/2}$ is relative to the SCE. The red dashed and solid blue lines correspond to the experimental pK_a and redox potentials. The black lines are the theoretical predictions.

does not change as much as in $Ru(OH)^+$ and the lowest minimum is still predicted to be a H-O—Ru-O1 dihedral angle of 0 degrees in solution (see Figure 3).

Solution Phase Calculations and Experimental Results. As a preliminary study to demonstrate that it is a useful exercise to construct a theoretical Pourbaix diagram, we have carried out calculations on the $Ru(OH_2)(bpy)(tpy)^{2+}$ complex studied by Takeuchi et al.[134] as a model for the monomer of the blue dimer catalyst. This complex differs from the Tanaka monomer only by the presence of the bipyridine ligand instead of the quinone ligand. The resulting theoretical Pourbaix diagram is shown in Supporting Information Figure S2, where it is compared to the experimentally derived one. The diagram for $Ru(OH_2)(bpy)(tpy)^{2+}$ has much simpler topology than that for the Tanaka's monomer (see Figure 1), so the present comparison provides an easily interpreted test of our theoretical approach. It is clear from Supporting Information Figure S2 that the theoretical prediction is topologically correct and accurate enough, with some deviation from experiment due to limitations of the model, to unambiguously assign all the species.

Relevant pK_a values and standard reduction potentials (E^0) were calculated in order to elucidate the complicated regions of the Pourbaix diagram for the Tanaka monomer (Figure 1). The theoretical Pourbaix diagram is presented in Figure 4 along with the data from Figure 1 through which $E_{1/2}$ lines are drawn and oxidation state and spin multiplicity assignments are made. The details of calculated pK_a and E^0 are summarized in Table 3. The calculated pK_a values for the proton dissociation of $Ru(OH_2)^{2+}$ and $Ru(OH)^+$ are seen to be 2.9 and 14.2, respectively, whereas they were reported to be 5.5 and 10.7, respectively, in the base titration measurements.

(134) Takeuchi, K. J.; Thompson, M. S.; Pipes, D. W.; Meyer, T. J. *Inorg. Chem.* **1984**, *23*, 1845–1851.

The top portion of the experimental diagram, i.e., $E_{1/2}$ > 250 mV, is assigned essentially the same as it was previously.[6] The lower portion of the diagram corresponding to the reduction of the quinone ligand is substantially revised. The one-electron-oxidized complex of $Ru^{II}(OH)^+$, doublet $Ru^{III}(OH)^{2+}$ assigned in the low pH (<3) and high potential (900−1100 mV) region (see Figure 5a), has a predicted pK_a of 4.3. Since this value is higher than that (pH 2.9) predicted for $Ru^{II}(OH_2)^{2+}$, the theoretical diagram predicts a horizontal line segment between pH 2.9 and 4.3 corresponding to the one-electron oxidation of $Ru^{II}(OH)^+$. Above pH 4.3, the theoretical diagram predicts a coupled one-proton, one-electron oxidation of $Ru^{II}(OH)^+$ to $Ru^{II}(O^{\bullet-})^+$. We should note that here we are describing the thermodynamics of some redox reactions that involve both electron and proton transfer, and we use the term proton-coupled electron transfer (PCET) in the thermodynamic sense that implies nothing about the corresponding kinetic pathways. On the other hand, the experimental data suggest a pK_a for $Ru^{III}(OH)^{2+}$ of ca. 2.7, whereas that of $Ru^{II}(OH_2)^{2+}$ is 5.5, in the opposite order from the predicted values. This implies a line segment with slope −118 mV/pH between pH 2.7 and 5.5 corresponding to the coupled two-proton, one-electron oxidation of $Ru^{II}(OH_2)^{2+}$ to $Ru^{II}(O^{\bullet-})^+$. The experimental data exhibit significant scatter in this region of the diagram, making it difficult to discern whether they fall on a line with slope −118 mV/pH in moving to lower pH from pH 5.5, but they definitely do not follow such a line below pH 4.4, where they appear to flatten out until they begin to follow the line segment with slope −59 mV/pH corresponding to the coupled one-proton, one-electron oxidation of $Ru^{II}(OH_2)^{2+}$ to $Ru^{III}(OH)^{2+}$ starting at pH 2.7. One possible explanation for such behavior would be that $Ru^{II}(O^{\bullet-})^+$ is a very reactive species at low pH, and abstracts a hydrogen atom from the small amount of CF_3CH_2OH present to form $Ru^{II}(OH)^+$ which in turn becomes protonated to form $Ru^{II}(OH_2)^{2+}$. This reaction might be so rapid that equilibrium in the oxidation of $Ru^{II}(OH_2)^{2+}$ is never established in this region.

We interpret the high pH region of the experimental diagram corresponding to the formation of the oxyl radical by deprotonation of $Ru^{II}(OH)^+$ in a similar way (see Figure 5b). Here the problem is exacerbated by the low solubility of the neutral complexes. As indicated previously, we assign the spectrum originally attributed to the $Ru^{II}(O^{\bullet-})(SQ)^0$ species to the $Ru^{II}(OH)(SQ)^0$ species on the basis of its calculated UV-vis spectrum and Ru—O bond length.[6] We would expect $Ru^{II}(O^{\bullet-})(SQ)^0$ to be even more reactive than $Ru^{II}(O^{\bullet-})(Q)^+$ because the latter (doublet) species is stabilized by the resonance structure $Ru^{IV}(=O)(SQ)^+$. Consequently, we do not indicate a line segment above the pK_a of $Ru^{II}(OH)^+$ corresponding either to the oxidation or reduction of $Ru^{II}(O^{\bullet-})(SQ)^0$. Unlike the behavior of the $Ru^{II}(O^{\bullet-})(SQ)^0$ oxyl radical in the Tanaka monomer, we believe that two oxyl radicals formed by deprotonation of the two hydroxo ligands in the binuclear Tanaka catalyst, $[(SQ)Ru^{II}(O^{\bullet-})$-$(O^{\bullet-})Ru^{II}(SQ)(btpyan)]^0$ (btpyan = 1,8-bis(2,2′:6′,2″-terpyrid-4′-yl)anthracene), react with each other to form an O—O bond en route to O_2 production.

Table 3. Calculated Values of pK_a, E^0, and $E_{1/2}$ at the density Functional Theory Level

reactions	predictions[a]
$Ru^{II}(OH_2)(Q)^{2+}_{(aq)} \leftrightarrow Ru^{II}(OH)(Q)^{+}_{(aq)} + H^{+}_{(aq)}$	$pK_a = 2.9$
$Ru^{II}(OH)(Q)^{+}_{(aq)} \leftrightarrow Ru^{II}(O^{\bullet-})(SQ)^{0}_{(aq)} + H^{+}_{(aq)}$	$pK_a = 14.2$
$Ru^{III}(OH)(Q)^{2+}_{(aq)} \leftrightarrow Ru^{II}(O^{\bullet-})(Q)^{+}_{(aq)} + H^{+}_{(aq)}$	$pK_a = 4.3$
$Ru^{II}(OH_2)(SQ)^{+}_{(aq)} \leftrightarrow Ru^{II}(OH)(SQ)^{0}_{(aq)} + H^{+}_{(aq)}$	$pK_a = 13.0$
$Ru^{II}(OH_2)(CatHH)^{2+}_{(aq)} \leftrightarrow Ru^{II}(OH_2)(CatH)^{+}_{(aq)} + H^{+}_{(aq)}$	$pK_a = -0.1$
$Ru^{II}(OH_2)(CatH)^{+}_{(aq)} \leftrightarrow Ru^{II}(OH_2)(Cat)^{0}_{(aq)} + H^{+}_{(aq)}$	$pK_a = 12.8$
$Ru^{IV}(=O)(Q)^{2+}_{(aq)} + e \leftrightarrow Ru^{II}(O^{\bullet-})(Q)^{+}_{(aq)}$	$E^0 = 1381$
$Ru^{III}(OH)(Q)^{2+}_{(aq)} + e \leftrightarrow Ru^{II}(OH)(Q)^{+}_{(aq)}$	$E^0 = 805$
$Ru^{II}(OH_2)(Q)^{2+}_{(aq)} + e \leftrightarrow Ru^{II}(OH_2)(SQ)^{+}_{(aq)}$	$E^0 = 475$
$Ru^{II}(O^{\bullet-})(Q)^{+}_{(aq)} + e \leftrightarrow Ru^{II}(O^{\bullet-})(SQ)^{0}_{(aq)}$	$E^0 = 220$
$Ru^{II}(OH)(Q)^{+}_{(aq)} + e \leftrightarrow Ru^{II}(OH)(SQ)^{0}_{(aq)}$	$E^0 = -119$
$Ru^{II}(OH_2)(SQ)^{+}_{(aq)} + e \leftrightarrow Ru^{II}(OH_2)(Cat)^{0}_{(aq)}$	$E^0 = -1001$
$Ru^{IV}(=O)(Q)^{2+}_{(aq)} + H^{+}_{(aq)} + e \leftrightarrow Ru^{III}(OH)(Q)^{2+}_{(aq)}$	$E_{1/2} = 1633 - 59.1 \times pH$
$Ru^{III}(OH)(Q)^{2+}_{(aq)} + H^{+}_{(aq)} + e \leftrightarrow Ru^{II}(OH_2)(Q)^{2+}_{(aq)}$	$E_{1/2} = 978 - 59.1 \times pH$
$Ru^{II}(O^{\bullet-})(Q)^{+}_{(aq)} + H^{+}_{(aq)} + e \leftrightarrow Ru^{II}(OH)(Q)^{+}_{(aq)}$	$E_{1/2} = 1058 - 59.1 \times pH$
$Ru^{II}(OH)(Q)^{+}_{(aq)} + H^{+}_{(aq)} + e \leftrightarrow Ru^{II}(OH_2)(SQ)^{+}_{(aq)}$	$E_{1/2} = 648 - 59.1 \times pH$
$Ru^{II}(OH_2)(SQ)^{+}_{(aq)} + 2H^{+}_{(aq)} + e \leftrightarrow Ru^{II}(OH_2)(CatHH)^{2+}_{(aq)}$	$E_{1/2} = -250 - 118.2 \times pH$
$Ru^{II}(OH_2)(SQ)^{+}_{(aq)} + H^{+}_{(aq)} + e \leftrightarrow Ru^{II}(OH_2)(CatH)^{+}_{(aq)}$	$E_{1/2} = -245 - 59.1 \times pH$
$Ru^{II}(OH)(SQ)^{0}_{(aq)} + H^{+}_{(aq)} + e \leftrightarrow Ru^{II}(OH_2)(Cat)^{0}_{(aq)}$	$E_{1/2} = -233 - 59.1 \times pH$

[a] E^o and $E_{1/2}$ are in units of mV relative to the SCE.

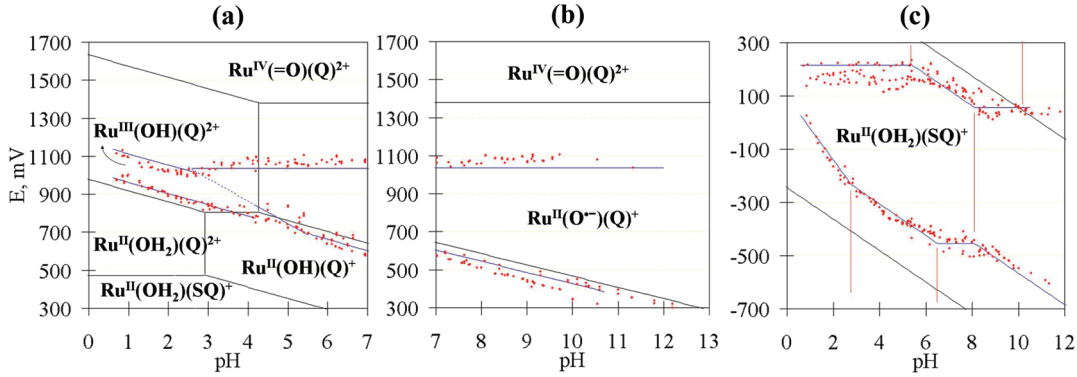

Figure 5. Blowups of sections of experimental and theoretical Pourbaix diagram of $Ru(OH_2)(Q)(tpy)^{2+}$. All features are as defined in Figure 4: (a) the low pH and high potential region; (b) the high pH region; and (c) the potential region below 200 mV.

In contrast to the previous proposed assignment of $Ru^{II}(OH_2)(Cat)^0$,[6] the "two-electron-reduced species of $Ru^{II}(OH_2)^{2+}$" in the potential region below 200 mV at low pH (see Figure 5c) is here reassigned as the singly reduced species $Ru^{II}(OH_2)(SQ)^+$ with a calculated pK_a of 13.0. The experimental value appears to be ca. 8.1. The one-electron standard reduction potential for singlet $Ru^{II}(OH_2)(Q)^{2+}_{(aq)} + 1e^- \leftrightarrow$ doublet $Ru(OH_2)(SQ)^{+}_{(aq)}$ is calculated to be 475 mV. Moving toward the more negative potential region, a coupled one-proton, one-electron transfer occurs as $Ru^{II}(OH_2)(SQ)^{+}_{(aq)} + H^{+}_{(aq)} + e^- \leftrightarrow Ru^{II}(OH_2)(CatH)^{+}_{(aq)}$, where the proton is bound to the O of Cat at the position adjacent to the water ligand. If the pH is acidic enough, coupled two-proton, one-electron transfer occurs as $Ru^{II}(OH_2)(SQ)^{+}_{(aq)} + 2H^{+}_{(aq)} + e^- \leftrightarrow Ru^{II}(OH_2)(CatHH)^{2+}_{(aq)}$. The first p$K_a$ of $Ru^{II}(OH_2)(CatHH)^{2+}$ is calculated to be -0.1 (experiment p$K_a = 2.9$), and the second pK_a to form singlet $Ru^{II}(OH_2)(Cat)^0$ is 12.8 (experiment p$K_a = 6.3$). The first pK_a of singlet $Ru^{II}(OH_2)(Cat)^0$ is calculated to be 18.1. Despite the quantitative differences in the pK_a and $E_{1/2}$ values between theory and experiment, the predicted topology of the lower portion of the Pourbaix diagram is entirely in accord with the experiment, including the horizontal line segment between pH 6.3 and 8.1 corresponding to the 1e-reducton of $Ru^{II}(OH_2)(SQ)^+$ (calc. pK_a = 13.0) to $Ru^{II}(OH_2)(Cat)^0$ (calc. $Ru^{II}(OH_2)(CatH)^+$ pK_a = 12.8). The experimental measurements around the pH 8−10.5 and 110 mV region indicate a flat line reflecting a one-electron reduction process. The theoretical prediction of a pK_a of 13.0 for $Ru^{II}(OH_2)(SQ)^+$, which is smaller than the 14.2 for $Ru^{II}(OH)(Q)^+$, is consistent with this observation.

The half-potential, $E_{1/2}$, of the coupled one-proton, one-electron transfer reaction $Ru^{II}(OH)(Q)^{+}_{(aq)} + H^{+}_{(aq)} + e^- \leftrightarrow Ru^{II}(OH_2)(SQ)^{+}_{(aq)}$ is predicted as $E_{1/2} = 648 - 59.1 \cdot$pH (in mV). Because the slope of the electrochemical potential for this PCET process was previously reported to be close to 30 mV/pH, we considered the coupled one-proton, two-electron transfer reaction $Ru^{II}(OH)(Q)^{+}_{(aq)} + H^{+}_{(aq)} + 2e^- \leftrightarrow Ru^{II}(OH_2)(Cat)^{0}_{(aq)}$, however, our calculations indicate that this reaction occurs at a much more negative potential. Moreover, the disproportionation reaction $2Ru^{II}(OH_2)(SQ)^{+}_{(aq)} \leftrightarrow Ru^{II}(OH)(Q)^{+}_{(aq)} + Ru^{II}(OH_2)(CatH)^{+}_{(aq)}$ is calculated to be endothermic and unlikely to occur. Our current detailed experimental investigation revealed no evidence of two-electron reduction coupled with protonation. Furthermore, radiolytic one-electron reduction of $Ru^{II}(OH_2)(Q)^{2+}$ using $CO_2^{\bullet-}$ at pH 3 and 7 produced species with identical visible spectra, presumably assigned as $Ru^{II}(OH_2)(SQ)^+$ as shown in Figure 6. This species decays exponentially with no dose dependence indicating that a disproportionation reaction does not take place.

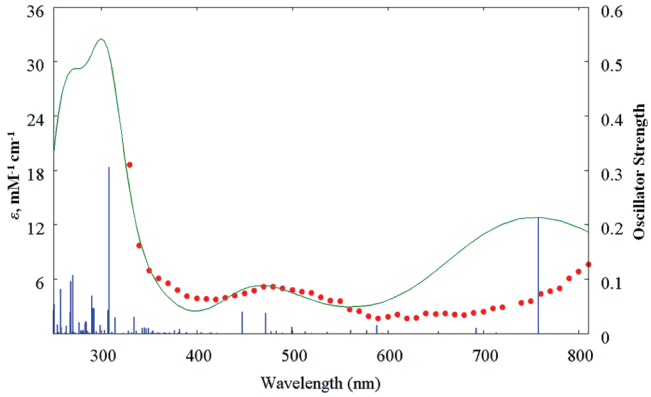

Figure 6. Pulse radiolysis measurements of $Ru(OH_2)(SQ)^+$ (red points, left *y*-axis) and the corresponding calculated UV−vis spectrum (green curve, blue impulses) at the TD-B3LYP/COSMO level of theory (right *y*-axis). The calculated peak at 756 nm is typically blue-shifted from the experimental semiquinone peak at ca. 900 nm.

Conclusions

The electronic states of the various oxidized and reduced species of the monomer of Tanaka's dinuclear Ru water oxidation catalyst produced by sequential deprotonation, electrochemistry, and pulse radiolysis have been calculated. The formal oxidation state of the metal center and each ligand has been systematically assigned despite frequent disagreement between DFT and ab initio electronic structure methods regarding spin multiplicity and electron distributions. The theoretical Pourbaix diagram for the $Ru(OH_2)(bpy)(tpy)^{2+}$ complex, the monomeric analogue of the blue dimer catalyst, was demonstrated to be topologically correct and accurate enough to unambiguously assign all the relevant species. The pK_a and standard reduction potential of selected complexes pertinent to the Tanaka monomer were calculated in order to generate a theoretical Pourbaix diagram for $Ru(OH_2)(Q)^{2+}$. The calculations provide a reasonable interpretation of the experimental results even for the challenging extreme experimental conditions of high pH and low solubility. The calculations predict $Ru^{II}(OH_2)(SQ)^+$ as the dominant species in the low potential region ($E < 250$ mV and pH < 8) instead of $Ru^{II}(OH_2)(Cat)^0$ as formerly assigned. The catecholate species appear at more negative potentials. In the high pH region, regardless of the applied potential, the reactive complexes, doublet $Ru^{II}(O^{\bullet -})(Q)^+$ and triplet $Ru^{II}(O^{\bullet -})(SQ)^0$, may undergo an H-atom abstraction reaction to become singlet $Ru^{II}(OH)(Q)^+$ and doublet $Ru^{II}(OH)(SQ)^0$, respectively. Despite the uncertainty in the solvation energy calculations, the predictions of the theoretical Pourbaix diagram still give a useful qualitative description for the interpretation of the experimental diagram. The consistency in predicting similar topology provides credibility for one-to-one electronic assignments from theoretical predictions to the various experimental conditions. This approach provides the possibility of assigning the even more complicated Pourbaix diagram for the anthracene-bridged Tanaka dimer catalyst.

Acknowledgment. The work at Brookhaven National Laboratory is funded under contract DE-AC02-98CH10886 with the U.S. Department of Energy and supported by its Division of Chemical Sciences, Geosciences, and Biosciences, Office of Basic Energy Sciences. Computational resources were provided by the National Energy Research Scientific Computing Center, which is supported by the Office of Science of the U.S. Department of Energy and the New York Center for Computational Sciences (New York Blue). We thank the U.S Department of Energy for funding under the BES Hydrogen Fuel Initiative.

Supporting Information Available: Explanation of torsional zero-point energy correction for $Ru(OH)^+$ complex, figure of H_2 dissociation at the CAS(2,2) level of theory, figure of experimental and theoretical Pourbaix diagram of $Ru(OH_2)(bpy)(tpy)^{2+}$, tables of Mullikan charge and spin density of various complexes, calculated Ru(O) (of water moiety) stretching frequencies and TD-DFT vertical excitation energies of the main intermediates, and tables of Cartesian coordinates of all intermediate species considered. This material is available free of charge via the Internet at http://pubs.acs.org.

IC900057Y